Non-Newtonian Pulsatile Blood Flow in a Curved Artery

H. Niazmand [1] and E. Ebrahimnia [1]

[1]*Department of Mechanical Engineering, Ferdowsi University of Mashhad*
Mashhad, Iran

Email: *hniazmand@yahoo.com*

ABSTRACT

Three-dimensional time-dependent incompressible Navier-Stokes equations are numerically solved in a body fitted coordinates system to study the pulsatile blood flow in a human aortic arch. A projection-type method is employed and to accelerate the numerical convergence of the flow field at each time step, two new pressure corrections are applied. First correction is based on the acceleration of the entry flow and the second one is designed to satisfy the continuity of mass fluxes in every cross section. A rescaled Newtonian model has been employed to predict the non-Newtonian blood behavior. Flow patterns in rescaled Newtonian fluid are studied in several section of the artery. The wall shear stresses, which are of much importance in the initiation of vascular diseases, are studied for both Newtonian and rescaled Newtonian fluid. The results indicated that inner regions close to the inlet of the aorta arch, with high wall shear stress values are vulnerable sites to the initiation and development of thrombus formation lesions which leads to atheroembolic stroke. On the other hand, regions with low values of WSS along the inner and outer walls are most susceptible to genesis of atherosclerosis disease. Present results indicate that the rescaled Newtonian model greatly influenced the axial velocity profiles and WSS distributions.

1. INTRODUCTION

Over the past decades, a large number of novel numerical methods have been proposed to analyze blood flow for understanding the relationship between vascular diseases and hemodynamics. Among the major challenges in blood flow computations are: the complex and variable geometry of the cardiovascular system; the complex and nonlinear material properties of the vessel walls; the pulsatile nature of blood flow; and the non-Newtonian viscous nature of blood [1]

In addition, it is also necessary to consider biological complexities in the analysis of blood flow with respect to diseases processes. Hemodynamic factors that have been suggested to be important in the initiation and development of vascular diseases are derived from the velocity field and involve several different forms, such as flow separation and vortex formation, shear stresses, and spatial and temporal shear stress gradients [2, 3]. It is well accepted that locations, where shear stresses are low or change rapidly in time and space are most vulnerable. These conditions are likely to prevail at places, where the vessel is curved, bifurcates, has a junction, side branch, or sudden change in flow geometry, and the flow is unsteady [2].

Aortic system is well known example of these vulnerable sites that is studied to understand the development of vascular diseases such as atherosclerosis and their dependence on flow structure [4-8]. Yet, most of the studies have considered blood as a Newtonian fluid. It is commonly assumed that the Newtonian model is a valid approximation for the rheological behavior of blood in large arteries. However, some investigations have shown that this is not a reliable assumption in some locations such as junctions, branches and curved arteries [9-12]. In general, blood behaves as a Newtonian fluid for high shear rate values, and as a non-Newtonian fluid for low values [12, 13]. Therefore, the non-Newtonian behavior must be considered in oscillatory flows, where the velocity gradient goes to zero at some part of the cycle during the period [2]. Also, it has been pointed out that in some diseased conditions such as patients with sever myocardial infarction, cerebrovascular diseases and hypertension, blood exhibits remarkable non-Newtonian properties [14].

Several authors have reported constitutive equations for the description of the shear thinning behavior of blood. In some studies Carreau–Yasuda model is used [15-20]. Sankar et al. [14] assumed blood as Casson fluid and Herschel–Bulkley fluid. Hernan et al. [21] employed Casson, Power-Law and Quemada models. In all studies significant differences in axial velocity profiles, secondary flows streamlines and WSS values between the non-Newtonian and

Newtonian fluid flows are revealed. Therefore a simple Newtonian fluid model for the blood may lead to false interpretation of experimental observations, particularly when complex vascular geometries are considered.

A standard constitutive equation is still not available which accurately describes the blood viscous properties under all flow conditions [15]. In order to predict the non-Newtonian behavior of blood, a rescaled Newtonian model is applied in the present study. The rescaled Newtonian flow is found to give reasonable representation of the non-Newtonian flow in most situations. [15-20].

2. METHOD

2.1 Geometry

The main systemic artery from the heart is the aortic arch, a 3D bend twisting about 180°, as shown in Fig. 1, which is adopted here as the flow geometry. The aorta is the main trunk of a series of vessels which convey the oxygenated blood to the tissues of the body for their nutrition. It is described in several portions, viz., the ascending aorta, the arch of the aorta, and the descending aorta, which last is again divided into the thoracic and abdominal aorta [7]. In the present study, according to the [7-9], the radius of the arch is set to 30 mm and the diameter of the vessel is assumed to be constant and equal to 24mm uniformly. The ascending and the descending aorta are considered 5 and 10 cm in length, respectively. The model neglects the main aortic branches and minor blood vessels leaving the aorta.

2.2 Rescaled Newtonian model

The shear thinning behavior of the blood has been approximated using a rescaled viscosity based on a characteristic shear rate ($\dot{\gamma}_c$) of the flow. However, there is no universally accepted definition of the characteristic shear rate. Some use the wall shear rate, which is often the highest shear rate occurring in blood flow [22, 23]. Others use the averaged shear rate in the artery, which has also been adopted in the present study [15-20].

$$\dot{\gamma}_c = \frac{4V}{D} \tag{1}$$

where V is the mean inlet velocity and D is the diameter of the artery.

To obtain the characteristic viscosity, η, the Carreau–Yasuda shear thinning model is used [16]:

$$\frac{\eta - \eta_\infty}{\eta_0 - \eta_\infty} = \left[1 + (\lambda \dot{\gamma}_c)^a\right]^{(n-1)/a} \tag{2}$$

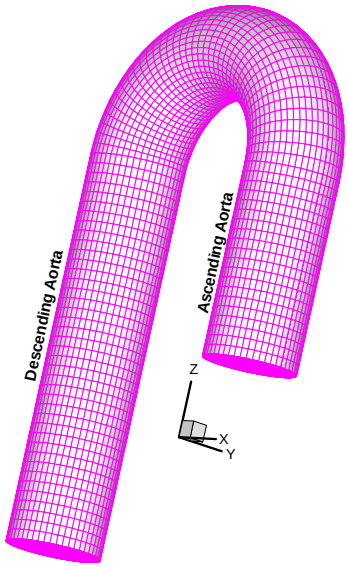

Fig.1. Aortic geometry and the coordinates system.

The parameters in Eq. (2) are obtained from experimental data provided by [16] as: $\eta_\infty = 2.2\times10^{-3}$ Pa.s, $\eta_0 = 22\times10^{-3}$ Pa.s, $\lambda = 0.11$ s, $a = 0.644$, $n = 0.392$ and $\rho = 1050 kg/m^3$.

2.3 The Governing Equations

The Governing Equations are the time-dependent incompressible Navier–Stokes equations in integral form as:

$$\iint \vec{V} \cdot d\vec{A} = 0 \tag{3}$$

$$\int_\forall \frac{\partial \vec{V}}{\partial t} d\forall + \iint \rho \vec{V}\vec{V} \cdot d\vec{A} = -\iint p\,\vec{n} \cdot d\vec{A} + \iint \mu \vec{\nabla}\vec{V} \cdot d\vec{A} \tag{4}$$

where ρ is the density of the fluid, $\vec{V}$ is the velocity vector, p is the pressure, and μ is the viscosity.

At the aortic inlet, a realistic pulsatile waveform was used based on experimental data reported by Pedley [24] as shown in Fig. 2. The Maximum velocity of cycle is 0.262 ms^{-1} and the Minimum velocity is -0.043 ms^{-1}. Zero gradients at the outlet are considered. Flow in the aorta is mainly laminar. For pulsating flow, turbulence may occur for a Reynolds number much larger that expected for steady flow. This is due to the fact that an accelerating flow is more stable than steady flow; also the decelerating flow is more unstable than steady flow. This can create bursts of turbulence during the decelerating phase [4]. Nerem et al. [25] found a critical Reynolds number for unsteady flows

in the form of $\mathrm{Re}_c = K \times \alpha$, where K is a constant ranging from 250 to 1000, and α is the frequency number defined as:

$$\alpha = R\left(\frac{2\pi}{Tv}\right)^{1/2} \tag{5}$$

where R is the artery radius, T = 1s is the period time of inlet flow pulse and ν is the kinematic viscosity of the fluid. In the present study the maximum α is about 16.47, and the maximum Re based on the maximum inlet velocity, $U_{\max}$, is much below the threshold Re_c.

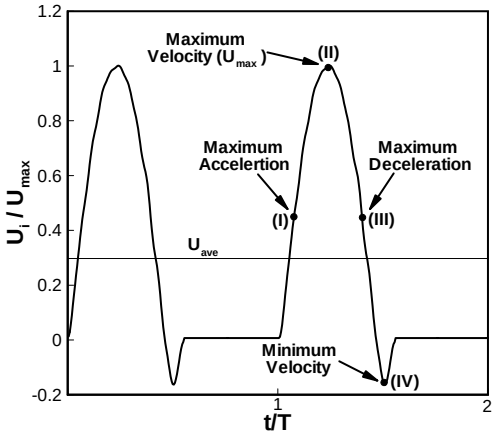

Fig.2. Dimensionless inlet velocity waveform and four important cycle positions.

2.4 The Numerical Algorithm

A projection-like method is used to solve the governing equations in generalized coordinates. The major problem during incompressible flow field solution appears to be the pressure term. It is well-known that the overall efficiency of a method for solving the incompressible Navier–Stokes equations largely depends on the approach adopted to solve a pressure correction equation such as Poisson equation. An accurate solution to the Poisson equation for incompressible flow can be too expensive in three dimensional forms. Following Dwyer et al. [26] two new pressure corrections are employed to improve the convergence performance of the Poisson equation solver. The corrections are based on the physical considerations of the inlet mass flow acceleration and preserving mass flow rate at each cross section.

The pressure correction, p', corresponding to the inlet mass flow acceleration is obtained according to the following expression:

$$-\frac{\partial p'}{\partial s} = \rho \frac{U_i(t+\Delta t) - U_i(t)}{\Delta t} \tag{6}$$

where U_i is inlet velocity and s is the streamline direction. The second pressure correction, p'', is obtained based on the local velocity defect as:

$$-\frac{\partial p''}{\partial s} = \rho \frac{\Delta U_k}{\Delta t} \tag{7}$$

where the local velocity defect at each cross section is defined as:

$$\Delta U_k = U_i - \frac{\iint_A \vec{V} \cdot d\vec{A}}{A} \tag{8}$$

where A is pipe cross sectional area.

The overall solution is obtained through the following procedure:

1- Determine the he time dependent pressure term, p', in each time step by solving the Eq.(6).
2- Solve the momentum equations with $p^n + p'$, where p^n is old pressure field.
3- Determine the local velocity defects and pressure correction p''.
4- Solve the momentum equations with the full pressure field, $p^n + p' + p''$.
5- Finally, solve the Poisson equation to obtain the new pressure field.

Using this method dramatically enhances the convergence rate in pulsatile flows.

3. RESULTS

3.1 Validations

The present numerical scheme has been compared with the results of Dwyer et al. [26] for an unsteady flow in an 180° curved pipe with ascending and descending parts. A sinusoidal inlet velocity waveform is considered for frequency number of 15. 3-D axial velocity profiles at a cross section located in the middle of the curve are compared in Fig. 3 for specified points on the inlet velocity waveform. Results show reasonable agreement with the maximum difference less than 6%.

3.2 Rescaled-Newtonian model results

A characteristic viscosity, η, based on Eq. 2, yields a value of 11.35×10^{-3} Pa s, which has been used in the evaluation of Re and frequency number, α.

Fig. 4a shows the sections and regions of interest in describing the flow patterns throughout the geometry. These sections are the aortic arch entrance (section B), mid way along the aortic arch (section C), aortic arch exit (section D), mid way along the descending aorta (section E) and descending aorta outlet (Section F). The 3-D axial velocity profiles at above sections

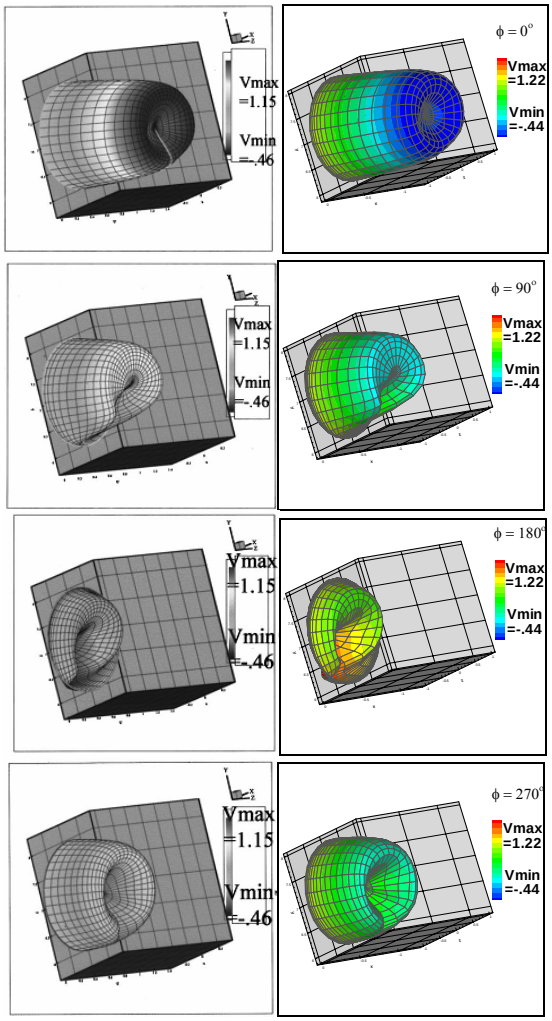

Fig. 3. Comparison of 3-D axial velocity profiles, left column [26], right column present results.

and important positions of the cycle corresponding to the points of: (I) maximum flow acceleration, (II) maximum flow velocity, (III) maximum flow deceleration, and (IV) minimum flow velocity (see Fig.2), are shown in Fig. 4b. The axial velocity profiles have been normalized with the maximum inlet velocity, $U_{\max}$, and rotated according to their actual position in the artery for more clarification.

The results demonstrate that for the time points with positive inlet velocity (I, II and III), the flow at the first half of aorta (cross-sections B and C) is skewed toward the inner aortic wall. This vortical type velocity profile has been induced due to the curvature of the geometry. Aortic curvature gradually changes the velocity profiles in sections C and D, resulting in an M-shaped velocity profile. Far downstream the aortic arc the flow is sharply skewed toward the outer wall of the aorta (cross-sections E and F).

In all sections, corresponding to the minimum velocity point (IV), velocity contours within the aorta exhibit different behavior from those at the other points in the cardiac cycle, due to the presence of major reverse flow.

Wall shear stress is likely the most relevant fluid mechanical parameter related to the initiation and development of some vascular diseases, which is presented in non-dimensional form as:

$$WSS = \left| \frac{R\,\tau_w}{\mu U_{\max}} \right| \qquad (9)$$

here, τ_w is the dimensional wall shear stress, R is the aortic radius, μ is the fluid dynamic viscosity and $U_{\max}$ is the maximum inlet velocity waveform.

The low and high wall shear stresses affect the histology and function of the endothelial cells in different ways. Exposure of the arterial wall to a relatively low wall shear stress may increase intercellular permeability and consequently increase the vulnerability of these regions to atherosclerosis [29]. On the other hand, high wall shear stresses and recirculation regions are believed to promote the thrombus formation, which is due to the rupture of a plaque or denudation of the endothelium overlying a fibrous plaque leading to atheroembolic stroke [4].

Fig. 5 shows the variations of WSS at the point of maximum inlet velocity waveform along the outer, inner and upper walls. Locations of these lines are shown in Fig. 4a.

The maximum value of WSS occurs inside the aortic arch, extending from 0.05 to 0.144m, along the inner wall close to the arch inlet. The spike occurs due to cross flow circulation towards the inner wall and shifting the point of local maximum velocity to the inner wall as can be seen from velocity profiles at sections B-II and C-II of Fig. 4b. The wall shear stress then shifts towards the outer wall as the flow progresses down-stream into the descending aorta. This shift in wall shear stress from the inner to the outer wall has also been confirmed by experimental observations [27, 28]. The region, where the shift occurs is expected to be a vulnerable location to plaque buildup. Figure also shows that the values of WSS in upper line are relatively higher along the aortic arch as compared to the other locations, which also makes the region more susceptible to plaque formation.

More information about the circumferential variations of WSS can be obtained from Figs. 6(a-c). In these figures the variations of WSS along the artery perimeter at three cross sections, B, C and D, inside the arch are plotted. For each cross section four important positions of the inlet velocity waveform, as shown in Fig. 2, are considered. Note

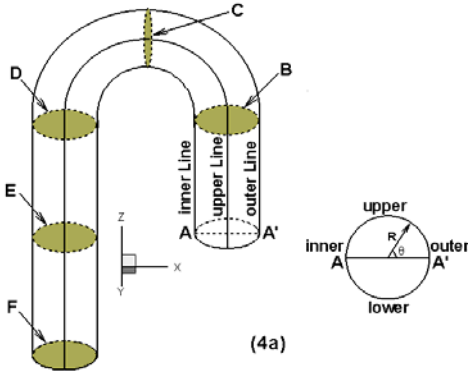

(4a)

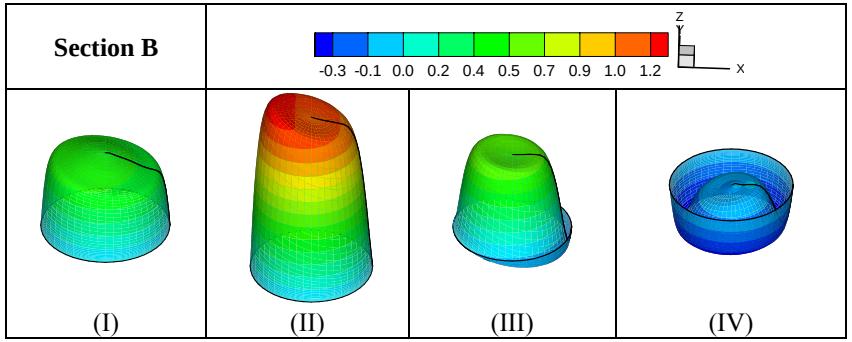

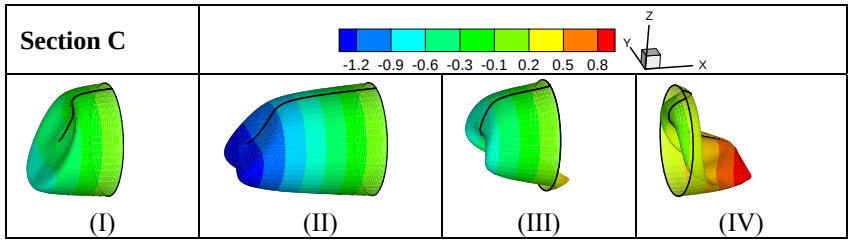

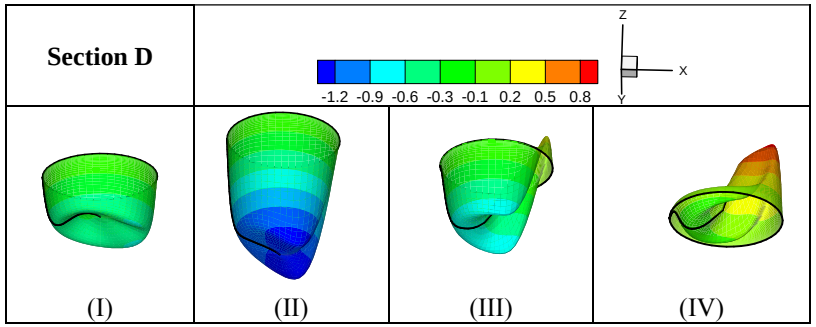

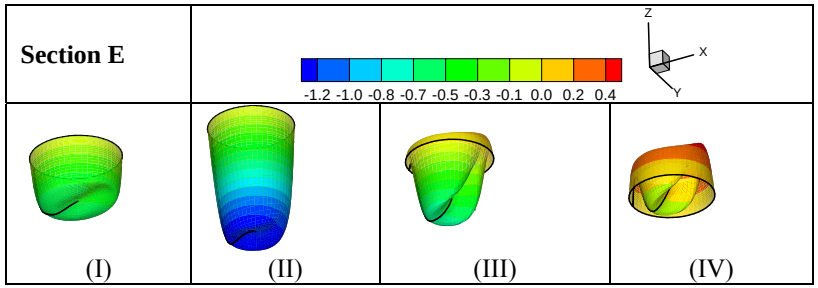

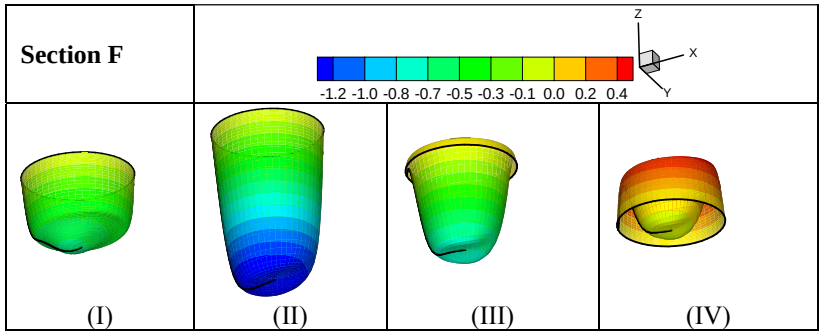

(4b)

Figs. 4(a-b). (a) Locations of the important cross sections and lines ,(b) 3-D axial velocity profiles at several cross sections and four cycle positions: (I) maximum acceleration, (II) maximum velocity, (III) maximum deceleration and (IV) minimum velocity .

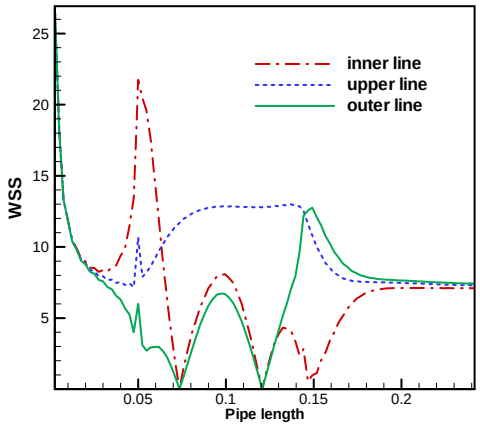

Fig. 5. Variations of WSS along the inner, outer, and upper lines at the maximum velocity point (II).

that $\theta = 0$ is located at the outer wall as shown in Fig. 4a. Fig. 6a, indicates that the maximum value of WSS at the inlet arch section occurs at inner wall ($\theta = 180^{o}$) at the maximum inlet velocity waveform, point (II), However, the maximum value of WSS shifts towards the upper and lower walls through the aortic arch (Fig. 6b and 6c). Also, note that the flow contains a symmetric plane located at $\theta = 180^{o}$ (A-A' plane in Fig. 4a) as indicated by symmetric behavior of WSS variations in the azimuthal direction.

Finally, the non-Newtonian behavior of the blood has been examined in Fig. 7. The rescaled Newtonian model has been compared with a Newtonian model at constant viscosity of 0.0035 Pas. Figure shows the axial velocity profiles, V_n, in the symmetric plane A-A' at cross section C, located in the middle of aorta. The comparison has been made for the maximum deceleration of inlet velocity waveform, point (III) in Fig. 2, corresponding to the lower shear rates, where the non-Newtonian behavior becomes more important. Figure shows that the velocity gradients at walls and the amount of reverse flow in Newtonian model are higher than rescaled Newtonian model.

Furthermore, the time averaged WSS during a cycle of inlet velocity waveform has been compared in Figs. 8a and b, for Newtonian and rescaled-Newtonian models, respectively. Comparing Fig 8a with 8b indicates that the two models predict almost similarly the regions of high risk, where WSS is either high or low. However, the Newtonian model predicts higher values for the maximum of time average of WSS than the rescale Newtonian model. Since, properly locating the vulnerable sites is of great practical importance developing of the reliable models for non-Newtonian behavior of blood becomes an issue. According to Figs. 8, the regions of high and low values of WSS are located around the inlet and outlet of the aortic arch at the inner and outer walls. Note that high values of the time

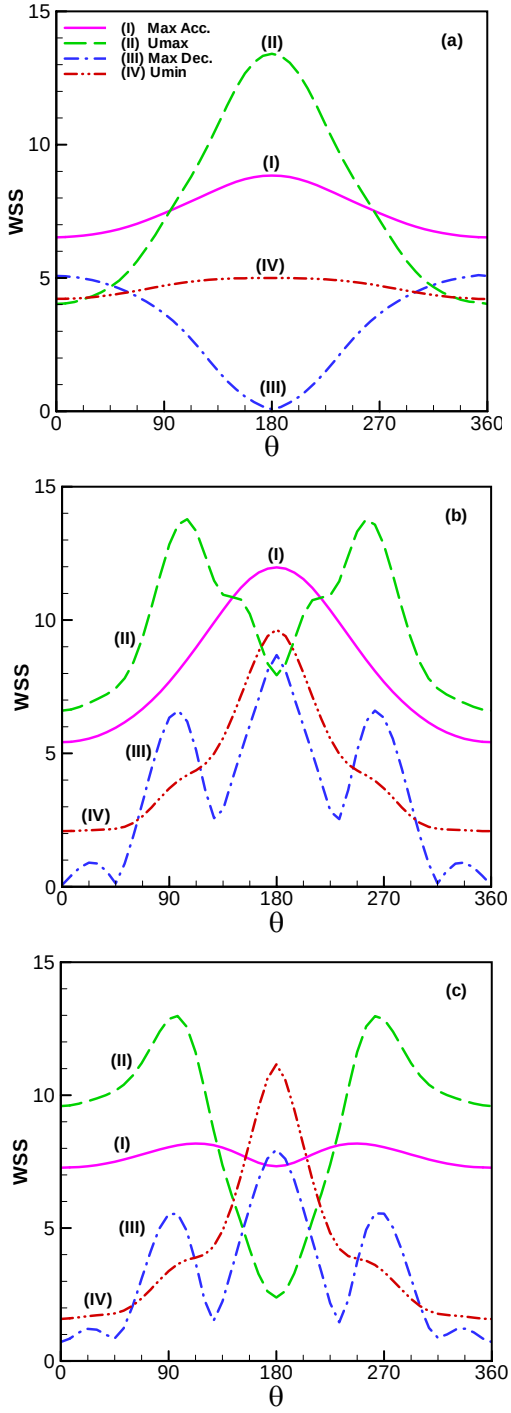

Figs. 6(a-c). Variations of WSS along the artery perimeter at four cycle positions and different cross sections: (a) cross section B, (b) cross section C, (c) cross section D.

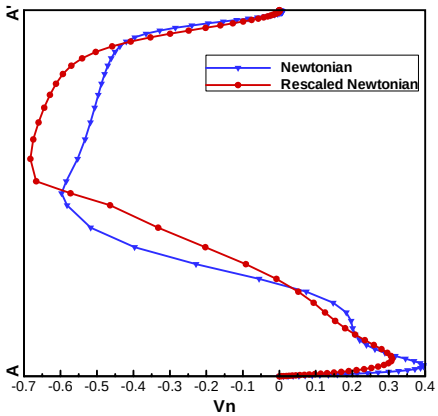

Fig. 7. Comparison of axial velocity in the symmetry plane (A-A') at section C for Newtonian and rescaled Newtonian model at the maximum deceleration of inlet velocity waveform, point (III).

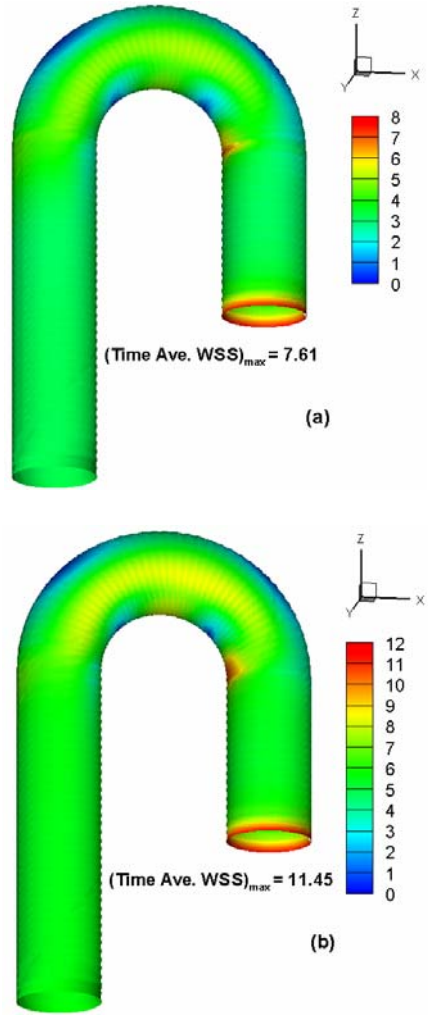

Figs. 8(a-b). Time averaged WSS contours, (a) rescaled-Newtonian model, (b) Newtonian model

averaged of WSS at the entrance region are due to stagnation of the flat inlet velocity profile at the artery walls.

CONCLUSIONS

The unsteady blood flow in an aortic artery is studied numerically. The computations are performed based on a slightly modified real geometry with a realistic inlet wave form. The convergence rate of the numerical method is enhanced through introducing two new pressure corrections. In order to predict the non-Newtonian blood behavior, a rescaled Newtonian model is employed. Comparing to the Newtonian model, significant differences in axial velocity profiles and WSS distributions are revealed. Present results indicate that vulnerable sites for genesis of atheroembolic disease are inner wall close to the inlet of the aorta arch. On the other hand, regions with low values of WSS along the inner and outer wall are most vulnerable to the initiation of atherosclerosis disease.

4. REFERENCES

[1] T. Yamaguchi, T. Ishikawa, K. Tsumota, Y. Imai, M. Nakamura and T. Fukui, Computational Blood Flow Analysis – New Trends and Methods, *Journal of Biomechanical Science and Engineering*, 1(1):29-50, 2006.

[2] A. Hernan, G. Rojas, Numerical implementation of viscoelastic blood flow in a simplified arterial geometry, *Medical Engineering & Physics*, 29:491–496, 2007.

[3] J. Suo, Investigation of blood flow patterns and hemodynamics in the human ascending aorta and major trunks o right and left coronary arteries using magnetic resonance imaging and computational fluid dynamics, Dissertation, Georgia Institute of Technology, January 2005.

[4] L. Morris, P. Delassus, A. Callanan, M. Walsh, F. Wallis, P. Grace and T. McGloughlin, 3-D Numerical Simulation of Blood Flow Through Models of the Human Aorta, *Journal of Biomechanical Engineering*, 127:767-775, 2005.

[5] T. Kim, A.Y. Cheer and H.A. Dwyer, A simulated dye method for flow visualization with a computational model for blood flow, *Journal of Biomechanics*, 37:1125–1136, 2004.

[6] M. Nakamura, S. Wada, T. Yamaguchi, Computational Analysis of Blood Flow in an Integrated Model of the Left Ventricle and the Aorta, *Journal of Biomechanical Engineering*, 128: 837-843, 2006.

[7] N. Shahcheraghi, H.A. Dwyer, A.Y. Cheer, A.I. Barakat and T. Rutaganira, Unsteady and Three-Dimensional Simulation of Blood Flow in the Human Aortic Arch, *Journal of Biomechanical Engineering*, 124:378-386, 2002.

[8] A. Leuprecht, S. Kozerke, P. Boesiger and K. Perktold, Blood flow in the human ascending aorta: a combined MRI and CFD study, *Journal of Engineering Mathematics*, 47:387–404, 2003.

[9] G.R. Cokelet, The rheology of human blood, In Biomechanics: Its Foundations and Objectives, pp. 63-103, PrenticeHall, 1981.

[10] J.H. Forrester and D.F. Young, Flow through a converging-diverging tube and its implications in occlusive vascular stenosis-I: Theoretical development, *Journal of Biomechanics*, 3:297-316, 1970.

[11] J.F. Stoltz, S. aillard and M. Lucuis, A study of the viscoelastic properties of blood in transient flow, *Journal of Biomechanics*, 13:341-346, 1980.

[12] J.C. Misra and B. Pal , A Mathematical Model for the Study of the Pulsatile Flow of Blood Under an Externally Imposed Body Acceleration, *Mathematical and Computer Modeling*, 29:89-106, 1999.

[13] G. Lorenzini, Blood velocity field numerical assessment using a GPL code in case of intravascular Doppler catheter affections: comparative analysis of different rheological models, *Journal of Biomechanics,* 38:2058–2069, 2005.

[14] D.S. Sankar and K. Hemalatha, Non-linear mathematical models for blood flow through tapered tubes, *Applied Mathematics and Computation,* 188:567–582, 2007.

[15] N. Bernard, R. Perrault and D. Coisne, Computational Approach to Estimating the Effects of Blood Properties on Changes in Intra-stent Flow, *Journal of Biomedical Engineering*, 34(8):1259–1271, 2006.

[16] F.J.H. Gijsen, E. Allanic, F.N. VandeVosse, and J.D. Janssen, The influence of the non-Newtonian properties of blood on the flow in large arteries: Unsteady flow in a 90° curved tube, *Journal of Biomechanics*, 32:705–713, 1999.

[17] F. J. H. Gijsen, F. N. Van de Vosse, and J. D. Janssen. The influence of the non-Newtonian properties of blood on the flow in large arteries: Steady flow in a carotid bifurcation, *Journal of Biomechanics*, 32:601–608, 1999.

[18] J. Chena, X.Y. Lua and W. Wangb, Non-Newtonian effects of blood flow on hemodynamics in distal vascular graft anastomoses, *Journal of Biomechanics*, 39:1983–1995, 2006.

[19] J. Chen and X.Y Lu., Numerical investigation of the non-Newtonian blood flow in a bifurcation model with a non-planar branch, *Journal of Biomechanics*, 37:1899–1911, 2004.

[20] J. Chen and X.Y Lu., Numerical investigation of the non-Newtonian pulsatile blood flow in a bifurcation model with a non-planar branch *Journal of Biomechanics*, 39:818–832, 2006.

[21] Pa. Neofytou, D. Drikakis, Non-Newtonian flow instability in a channel with a sudden expansion, *Journal of Non-Newtonian Fluid Mechanics*, 111:127–150, 2003.

[22] D.E. Mann, J.M. Tarbell, Flow of non-Newtonian blood analog fluids in rigid curved and straight artery models, *Biorheology*, 27:711–733, 1990.

[23] Y.I. Cho and R. Kensey, Effects of the non-Newtonian viscosity of blood flows in a diseased arterial vessel, Part 1: steady flows, *Biorheology,* 28:241–262, 1991.

[24] T.J. Pedley, The Fluid Mechanics of Large Blood Vessels, Cambridge University Press; 1980.

[25] R. M. Nerem, W. A Seed and N. B. Wood, An experimental study of the velocity distribution and transition to turbulence in the aorta, *Journal of Fluid Mechanics*, 52:137–160, 1972.

[26] H. A. Dwyer, A. Y. Cheer, T. Rutaginira and N. Shahcheraghi, Calculation of Unsteady Flows in Curved Pipes, *ASME Journal of Fluids Engineering*, 123:869–877, 2001.

[27] T. L. Yearwood, and K. B. Chandran, Physiological Pulsatile Flow Experiments in a Model of the Human Aortic Arch, *Journal of Biomechanics*, 15(9):683–704, 1984.

[28] V. S. Choi, L. Talbot, and I. Cornet, Experimental Study of Wall Shear Rates in the Entry Region of a Curved Tube, *Journal of Fluid Mechanics*, 93:229–274, 1979.

[29] T. Ohashi, Remodeling of vascular endothelial cells exposed to fluid shear stress: experimental and numerical approach, *Fluid Dynamics Research*, 37:40–59, 2005.